

Forecasting vegetation condition for drought early warning systems in pastoral communities in Kenya

Adam B. Barrett^{a,b}, Steven Duivenvoorden^{a,c}, Edward Salakpi^a, James M. Muthoka^d, Seb Oliver^{c,a} and Pedram Rowhani^{d*}

^a *The Data Intensive Science Centre, Department of Physics and Astronomy, University of Sussex, Brighton BN1 9QH, UK*

^b *Sackler Centre for Consciousness Science, Department of Informatics, University of Sussex, Brighton BN1 9QJ, UK*

^c *Astronomy Centre, Department of Physics and Astronomy, University of Sussex, Brighton BN1 9QH, UK*

^d *School of Global Studies, Department of Geography, University of Sussex, Brighton, BN1 9QJ, UK*

Corresponding author: P.Rowhani@sussex.ac.uk

Abstract

Droughts are a recurring hazard in sub-Saharan Africa, that can wreak huge socioeconomic costs. Acting early based on alerts provided by early warning systems (EWS) can potentially provide substantial mitigation in terms of money and lives lost. However existing EWS tend only to monitor, rather than forecast, the environmental and socioeconomic indicators of drought, and hence are not always sufficiently timely to be effective in practice. Here we make a first attempt at forecasting satellite-based indicators of vegetation condition that are commonly monitored. Specifically, we forecast the Normalized Difference Vegetation Index (NDVI) and the Vegetation Condition Index (VCI) over pastoral livelihood zones in Kenya as these are the common indicators used by the National Drought Management Authority (NDMA). Using data from MODIS and Landsat, we apply linear autoregression and Gaussian processes modeling methods and demonstrate accurate forecasting several weeks ahead. We explored predicting the drought alert marker used by NDMA ($3 \text{ month VCI} < 35$). Both of our models were able to predict this alert marker four weeks ahead

with a hit rate of around 89% and a false alarm rate of around 4%, or 81% and 6% respectively six weeks ahead. The methods developed here can identify a deteriorating vegetation condition well in advance and thus help disaster risk managers act early to support vulnerable communities and limit the impact of a drought hazard.

Keywords: Landsat; MODIS; Gaussian Processes; Drought; NDVI; VCI

¹ 1. Introduction

² Droughts are a major threat globally as they can cause substantial damage
³ to society, especially in regions that depend on rain-fed agriculture. They par-
⁴ ticularly impact food security by significantly reducing agricultural production
⁵ (Lesk et al., 2016) and raising food prices (Nelson et al., 2014; Brown and Kshir-
⁶ sagar, 2015), which often leads to increased levels of malnutrition, migration,
⁷ disease, and other health concerns (Piguet et al., 2011; Stanke et al., 2013).
⁸ Since 2000, there have been 319 drought events reported (EMDAT 2019), which
⁹ together have killed over 21,000 people and affected almost 1.4 billion others.
¹⁰ The majority of these events took place in sub-Saharan Africa where many
¹¹ communities rely on predictable rainfall patterns for their livelihood.

¹² In East Africa, the main economic activity in the arid and semi-arid lands
¹³ (ASAL) is subsistence rain-fed agriculture, as well as livestock farming using
¹⁴ pastures and grasslands as the main source of fodder. The pastoral and agro-
¹⁵ pastoral communities who live in these drylands have dealt with rainfall vari-
¹⁶ ability and drought over centuries by developing extensive adaptation and mit-
¹⁷ igation strategies to reduce their vulnerability to these shocks (Nyong et al.,
¹⁸ 2007; Orindi et al., 2007). However, in recent years these communities have
¹⁹ seen their coping strategies compromised by population growth and land use
²⁰ change (Galvin et al., 2001). Additionally, while there is some uncertainty in
²¹ the climate models (IPCC, Stocker et al., 2013), rainfall variability is expected

²² to increase in the region (Tierney et al., 2015; Yang and Huntingford, 2018).
²³ These factors in combination will make it harder for indigenous knowledge sys-
²⁴ tems to deal with droughts, and exacerbate the problems created by droughts.
²⁵ Governments and donor agencies in the region have thus developed several tools
²⁶ and early warning systems (EWS) to mitigate the impact of droughts on pas-
²⁷ toralists.

²⁸ Most EWS tend to monitor current key biophysical and socio-economic fac-
²⁹ tors to assess the possible exposure of vulnerable people to specific hazards.
³⁰ However, once the impacts are visible, it will be too late to mitigate the con-
³¹ sequences (Kogan et al., 2013). Additionally, being better prepared before a
³² drought hits significantly reduces the costs and losses from these disasters (Ven-
³³ ton et al., 2012). Hence, EWS now increasingly include expert knowledge and
³⁴ qualitative assessments of seasonal climate forecasts to assess the future develop-
³⁵ ment of food security, and define actions to mitigate possible losses (Coughlan de
³⁶ Perez et al., 2015; Tozier de la Poterie and Baudoin, 2015).

³⁷ Within East Africa, the Famine Early Warning Systems Network (FEWS
³⁸ NET) monitors food security through data collection and a deep understand-
³⁹ ing of the livelihood patterns in the region. A team of experts and analysts
⁴⁰ will also look at seasonal climate forecast to estimate future food security out-
⁴¹ comes using scenario development (FEWS-NET, 2018). In Kenya, the drought
⁴² EWS operated by the National Drought Management Authority (NDMA) pro-
⁴³ vides monthly bulletins assessing food security in the 23 ASAL regions based on
⁴⁴ environmental (rainfall, vegetation condition) and socio-economic (production,
⁴⁵ access, and utilisation) factors. Based on these factors, the bulletins include
⁴⁶ a qualitative evaluation of food security outcomes in the months ahead. How-
⁴⁷ ever, EWS should move from forecasting hydro-meteorological events toward
⁴⁸ estimating the expected consequences of hazards, i.e. impact-based forecasting,

⁴⁹ to identify more effective early action protocols (WMO, 2015; Sai et al., 2018).

⁵⁰ Pastoralists strongly rely on forage availability to keep their livestock. Existing EWS use satellite-based earth observation data to provide information on pasture condition through the use of vegetation indices and other satellite-derived drought indices, such as the Normalized Difference Vegetation Index (NDVI) and the Vegetation Condition Index (VCI, Kogan, 1995; Klisch and Atzberger, 2016; Rulinda et al., 2011; Rojas et al., 2011). These products are commonly used as drought indicators as they provide timely and regular assessment of vegetation health over large spatial areas. EWS should include a forecast of these indicators as it would allow local and national stakeholders to act early and support the pastoralists in times of drought. Recent studies have highlighted the potential of satellite-based earth observation data to forecast agricultural productivity (Zambrano et al., 2018) and seasonal forage availability (Vrieling et al., 2016).

⁶³ The main goal of this paper is to explore two novel methods to forecast the vegetation indices that are commonly used in the pastoral areas of Kenya to monitor droughts. We specifically aim to estimate the potential to forecast NDVI and the 3-month VCI (VCI3M), as used by the NDMA in their monthly bulletins, in pastoralist areas up to six weeks ahead, using Gaussian Process regression (GP, Rasmussen and Williams, 2006) with data derived from the Landsat mission (every 16 days at 30 m resolution), and linear autoregressive (AR) modelling (e.g. Hamilton, 1994) applied to data from the MODerate resolution imaging Spectroradiometer (MODIS - daily data at 500 m resolution). GP regression uses kernel-based non-parametric Bayesian inference on the structure of correlations between data points, and is widely applied to classification, interpolation, change detection and forecasting problems (Brahim-Belhouari and Vesin, 2001; Chandola and Vatsavai, 2011; Camps-Valls et al., 2016; Upreti et al.,

76 2019). For an overview on the principles of GPs, and how they have previously
77 been applied throughout remote sensing, see Camps-Valls et al. (2016). Linear
78 AR is the regression of future observations on past observations, assuming a
79 linear dependence. This has previously been performed on monthly (i.e. tem-
80 porally more sparse) NDVI data, see for example Asoka and Mishra (2015)
81 and Papagiannopoulou et al. (2017), with mixed results in terms of forecasting
82 potential (R^2 -scores between 0 and 0.4 at a lead time of one month).

83 **2. Study area**

84 About 80% of Kenya lies within the ASALs, and the main economic activity
85 in these regions is livestock farming (UNDP, 2013; FAO, 2014). The livestock
86 sector accounts for 13% of the national GDP and 43% of its agricultural GDP.
87 Pastures and grasslands in the ASAL serve as the main source of fodder for the
88 pastoral communities in Kenya Behnke and Muthami (2011). Following several
89 periods of intense drought, the government in Kenya established the NDMA in
90 2016, to set up and operate a drought early warning system (DEWS), as well
91 as to establish drought preparedness strategies and contingency plans (GoK).
92 One key biophysical indicator used by the NDMA drought phase classification
93 is the VCI (Klisch and Atzberger, 2016), which is measured at county level as
94 well as over the different livelihood zones within the county (FEWS NET 2011).
95 This study focused on the 10 (agro)-pastoral livelihood zones (see Fig 1), which
96 cross 15 counties. The names of the 29 livelihood zone county intersections can
97 be found in Appendix Appendix C. FEWS NET shape files were used to define
98 these regions, and to demarcate the Landsat and MODIS pixels from which to
99 sample data.

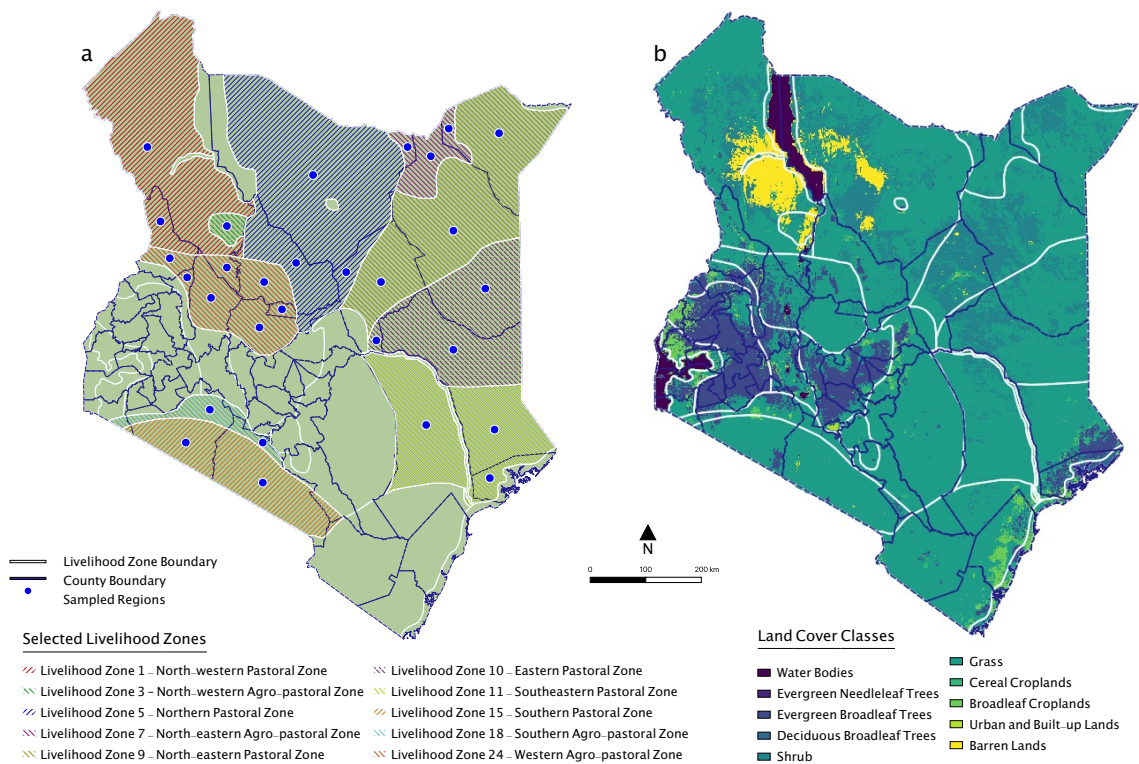


Figure 1: Maps of Kenya showing (A) the livelihood zones from which pixels were sampled for analysis, and (B) land cover classification (according to the MODIS MCD12Q1 map). Analyses were performed for 29 regions, defined by pastoral livelihood zone and county intersections. For the MODIS data only those pixels identified as being from grassland are used.

100 **3. Data**

101 *3.1. Landsat*

102 Landsat-5, 7 and 8 (Roy et al., 2014) red and near infrared (NIR) surface
103 reflectances and quality assessment (QA) data from the 10 pastoral livelihood
104 zones of Kenya, from 1/1/2000 to 1/2/2019, were obtained using the United
105 States Geological Survey (USGS) EarthExplorer. Specifically, data were drawn
106 from the Level-1 Precision Terrain (L1TP) processed dataset, which has well-
107 characterized radiometry and is inter-calibrated across the different Landsat
108 sensors. The QA data indicate whether or not each observation is affected by
109 cloud, we only select pixels classified as clear. The spatial resolution of these
110 data is 30m and the repeat interval is 16 days. Landsat-5 data were available
111 up until November 2011 (albeit with several large gaps), Landsat-7 data were
112 available for the whole time-period, and Landsat-8 data were available from
113 March 2013.

Red and NIR observations were combined to obtain NDVI, according to the formula

$$\text{NDVI} = \frac{\text{NIR} - \text{red}}{\text{NIR} + \text{red}}. \quad (1)$$

114 We note that the red and NIR bands are defined by slightly different spectral
115 ranges for the different Landsat missions, and that this can lead to slightly
116 different NDVI values for the same vegetation. More specifically, Landsat-8
117 measures slightly higher values for the NDVI of dry shrub-lands than Landsat-7,
118 while at higher values of NDVI there is more convergence (Dandan Xu, 2014).
119 The data from all three Landsat missions where used to train the GP's (see
120 Section 4).

121 Landsat data is acquired in tiles that slightly overlap. Where there was over-
122 lap, both observations were retained, since the methods employed can handle
123 multiple observations from the same time-point. We note that two observations

¹²⁴ of an overlap area taken on the same day are highly correlated but not identical,
¹²⁵ due to noise (NDVI values obtained from pixels sampled twice exhibit between
¹²⁶ them an R^2 -score of 0.76; see equation 7 for definition of R^2 -score).

¹²⁷ From each of the 29 pastoral livelihood zone and county intersections (see
¹²⁸ Fig. 1), 1 000 random pixels were selected for analysis. It was sufficient to use
¹²⁹ only 1 000 pixels per region as the R^2 -score comparing the average time series of
¹³⁰ all pixels from a region with the average of 1 000 random pixels was 0.9993. For
¹³¹ averaging over 100 random pixels the R^2 -score against averaging over all pixels
¹³² was 0.989, indicating that 100 pixels is sufficient for doing regional forecasting.
¹³³ A maximum of around 500 observations over time was obtained for each pixel,
¹³⁴ however for many pixels the total number of observations was a lot less than
¹³⁵ this due to cloud cover (there was also a lot of missing Landsat-7 data due to
¹³⁶ a permanent failure of the scan line corrector for Enhanced Thematic Mapper
¹³⁷ Plus on 31st May 2003). Pixels with fewer than 250 good observations during
¹³⁸ the 19 year observation period (i.e. less than $\sim 50\%$ of possible observations)
¹³⁹ were not selected for analysis (except for some regions for which this threshold
¹⁴⁰ had to be dropped to 180 observations in order to be able to obtain 1 000 pixels,
¹⁴¹ see Table C.6 in the Appendix).

¹⁴² *3.2. MODIS*

¹⁴³ Analogous data were also obtained from the MODIS Terra/Aqua Nadir
¹⁴⁴ BRDF-Adjusted Reflectance (NBAR) product (MCD43A4,v006; Schaaf and
¹⁴⁵ Wang, 2015) via the NASA Land Processes Distributed Active Archive Center
¹⁴⁶ (LP DAAC) using AppEEARS.¹ The spatial resolution of these data is 500m
¹⁴⁷ and the repeat interval is 1 day. From each of the 29 pastoral livelihood zone
¹⁴⁸ and county intersections, 100 random pixels were selected for analysis, out of

¹The Application for Extracting and Exploring Analysis Ready Samples (AppEEARS).

149 those pixels identified as being from grassland according to the MODIS land
150 cover classification maps (MCD12Q1,v006), this last step was not done for the
151 Landsat data.

152 **4. Methods**

153 *4.1. Temporal gridding and gap-filling*

154 To prepare the datasets for the testing of forecasting, each NDVI time series
155 was processed into a form containing, wherever possible, precisely one obser-
156 vation every 7 days. For the MODIS data, this required taking the mean of
157 all reliable daily observations each week. For the Landsat data, this required
158 compilation and interpolation of data sampled every 16 days from up to 3 dif-
159 ferent Landsat missions. Further, gap-filling had to be carried out on both
160 datasets whenever there was a lack of reliable observations due to cloud cover
161 and/or instrumental malfunction. Interpolation of gaps was vital for accurate
162 construction of NDVI anomaly and VCI from raw NDVI, since calculation of
163 these requires the raw NDVI values for the corresponding week in every year
164 of the recording, see Section 4.2. Further, for AR forecasting (Section 4.5.2),
165 lengthy segments of regular gridded data must be input for good model param-
166 eter estimation. There is a choice of methods for gap-filling (Kandasamy et al.,
167 2013), and these fall into the categories of temporal interpolation and spatial in-
168 terpolation. Temporal interpolation was chosen given that spatial interpolation
169 methods suffer from the fact that there are frequently clouds over Kenya that
170 cover large groups of neighbouring pixels. The following subsections describe
171 respectively the gridding and gap-filling methods employed on the Landsat and
172 MODIS data, and compare the performance of these methods with alternatives.

¹⁷³ 4.1.1. *Gridding and gap-filling on Landsat data using Gaussian Processes*

Gridding and gap-filling on the Landsat data was done using Gaussian Processes (GP). A Gaussian Process is a probabilistic model defined as a collection of random variables for which any finite subset has a joint Gaussian distribution Rasmussen and Williams (2006). Formally, for an output y and inputs \mathbf{x} :

$$f(\mathbf{x}) \sim \mathcal{GP}(m(\mathbf{x}), k(\mathbf{x}, \mathbf{x}')), \quad (2)$$

$$y_i = f(\mathbf{x}_i) + \sigma_r, \quad (3)$$

¹⁷⁴ where the mean function $m(\mathbf{x})$ represents the expectation $E[f(\mathbf{x})]$ and the kernel
¹⁷⁵ function $k(\mathbf{x}, \mathbf{x}')$ defines the covariances $\text{cov}(f(\mathbf{x}), f(\mathbf{x}'))$, which specifies how
¹⁷⁶ similar outputs $f(x)$ and $f(x')$ are. The sample drawn from $f(\mathbf{x})$ at locations
¹⁷⁷ $\mathbf{x}_{n=1}^N$ follow a joint multivariate Gaussian with covariance matrix determined
¹⁷⁸ by the kernel function. Here we have that the \mathbf{x}_i are the dates, t_i , of the
¹⁷⁹ observations, and y_i is the NDVI at time t_i , subject to measurement error σ_r .
¹⁸⁰ To interpolate, the existing data were used to fit the mean m and the kernel k ,
¹⁸¹ and then the GP with the fitted mean and kernel provided an estimate of the
¹⁸² probability distribution for the missing data.

For $m(t)$ the mean of the data was taken. To determine the kernel, compositional Kernel Search (Duvenaud et al., 2013) was used to determine the best kernel combination, by calculating the maximum evidence² (Marginal likelihood) for any product or sum of two common kernel combinations (Linear, Radial Basis Function, Periodic, Rational Quadratic and Matrn). The kernel with the highest evidence for Landsat NDVI time series in Kenya is the Radial Basis Function (RBF) in addition to the Periodic kernel ($k_{RBF} + k_P$) where the

²In practice the evidence lower bound (ELBO) was used instead of the evidence (p_σ) with $\log(p_\sigma) \geq \text{ELBO}$

period p was set to one year:

$$k_{RBF}(t, t') = \sigma_{RBF}^2 \exp\left(-0.5 \frac{|t - t'|^2}{l_{RBF}^2}\right), \quad (4)$$

$$k_P(t, t') = \sigma_P^2 \exp\left(-2 \frac{\sin^2(\pi|t - t'|/p)}{l_P^2}\right). \quad (5)$$

183 This GP contains 5 parameters to be fit ($\sigma_r, \sigma_{RBF}, l_{RBF}, \sigma_P, l_P$), which were
184 learned using Stochastic Variational Inference (SVI). The code was written using
185 the Deep Universal Probabilistic Programming language from **Pyro**, which is
186 written in **Python** and supported by **PyTorch**.

187 This interpolation method was used to predict a NDVI value for each pixel
188 every Saturday from 1/1/2000 until 2/2/2019, and thus obtain time series with
189 regular weekly observations. Thus the processed, gap-filled, time series have
190 distinct observation dates from the raw data, which consisted of observations
191 from up to 3 different Landsat missions, each at 16 day temporal resolution.³

192 Two versions of GP gap-filling were carried out, which we refer to as forecast
193 mode and non-forecast mode. For the non-forecast mode all the data (1/1/2000
194 to 1/2/2019) from a single pixel were used to train the GP to fill in all the
195 gaps, using both the periodic and RBF kernel. The non-forecasting mode was
196 used as the “ground truth” to test forecasts against in Section 5. The forecast
197 mode, by contrast, only used past data for both extrapolation (forecasting) and
198 interpolation - when doing forecasting with a near real-time data stream, one
199 of course does not have access to future data.

³Technically this means that when forecasting with this method, for a given lead time, the actual time between the last observation and the forecasted observation will vary from week to week.

200 *4.1.2. Gridding and gap-filling on MODIS data*

201 As mentioned above, gridding of the MODIS data was done by taking the
202 mean of all reliable daily observations each week. Gaps in the MODIS data were
203 then filled using temporal quadratic interpolation. Quadratic interpolation fills
204 each gap using the best fit quadratic function to the two points before the gap
205 and the two points after the gap (via least squares).⁴ In tests, it was found
206 that quadratic interpolation performed favourably compared to other methods
207 on these data, including GP (unlike for Landsat, see Section 4.1.3 below). The
208 SavitzkyGolay (SG, Savitzky and Golay, 1964) smoothing method was then
209 used to filter high-frequency measurement noise. SG smoothing involved, for
210 each data point, fitting a polynomial to a window centred on the data point, and
211 then replacing that data point with the corresponding point on the polynomial
212 fit. The polynomials were fit, for each window, to the original data. Based on
213 previous applications of this method to smoothing MODIS data (Kandasamy
214 et al., 2013; Chen et al., 2004), sliding windows of length 7 time-steps (weeks)
215 and a polynomial of order 2 (i.e. quadratic function) were chosen, and fitting
216 done using least squares. Note that smoothing was not required after gap-filling
217 in the Landsat data with GPs, since the kernel function used for GPs already
218 enforce a smooth function.

219 Since there were occasional long segments of interpolated data, where large
220 gaps had been filled, and NDVI values sometime took unrealistic values (greater
221 than 1 or less than 0), it was decided to remove all interpolations above a
222 maximum length, L_{\max} .⁵ In choosing L_{\max} , a trade off between quality and
223 quantity of remaining data points had to be made. The choice $L_{\max} = 6$ was

4When gaps were longer than 6 weeks, the interpolation was not trusted, and the gaps were reinserted after smoothing, and before carrying out forecasting, see Section 4.5.2.

5This was not an issue for the Landsat data, since the GP interpolations derive from the entire time series, and values within a long interpolation take values close to the mean for the time of the year.

made, after exploring a range of values and finding results to be not sensitive to the precise choice within the range between 4 and 8 (see Table C.5. This meant that all interpolated data points were no more than 3 weeks distant from a real observed data point, which is within the range for which interpolation can be assumed to be reasonably accurate, given the forecasting results found (see Section 5).

4.1.3. Comparison of other possible gap-filling methods

The performance of the gap-filling methods employed, compared with alternatives, was tested by removing observations, applying the method, and then comparing the interpolated points with the removed points. GP interpolation and linear, quadratic and cubic polynomial interpolation methods were tested, on both the Landsat and MODIS datasets. An example of the pixel level interpolation on Landsat data can be found in Appendix A.8. R^2 -scores were obtained for using the interpolated values to predict the “true” values for the missing data points.

For the Landsat data, one randomly chosen point between 1/1/2014 and 1/2/2019 was removed from 2000 randomly selected individual pixel time series.⁶ For the MODIS data, 1200 randomly selected NDVI time series (1/1/2014 to 1/2/2019) were sampled from 26 livelihood zone and county intersections. 20 randomly selected NDVI values were dropped from each of the time series and the various gap-filling methods were used to interpolate the dropped values. The results for Landsat are shown in Table 1 and for MODIS in Table 2.

For the Landsat data, the GP method achieved the highest R^2 -score, thus showing its utility, and justifying our choosing it. The R^2 -score of 0.67, achieved

⁶We remove the mean of the individual NDVI time series for every single observed and interpolated datum before calculating the R^2 -scores. This avoids an over-estimate of the denominator (see Equation 4) due to the variance from different regions in Kenya. This also forces the mean value prediction to be zero, which it should be for a R^2 calculation.

Table 1: R^2 -scores of pixel level NDVI for different commonly used interpolation methods and our GP method for Landsat data. At the pixel level a random data point was removed, and then interpolated with the methods in column 1 of the table. The second column gives the R^2 -scores if both past and future data is used for the interpolation, and the third column gives the R^2 -scores if only past data is used (i.e. one is extrapolating). The numbers in parentheses show the R^2 -scores when unrealistic NDVI values ($NDVI > 1$ or $NDVI < 0$) are removed.

Method	Interpolation	Forecast extrapolation
GP	0.67	0.56
Linear	0.53	-6.68 (-0.74)
Quadratic	-0.07 (0.14)	(-3.86)
Cubic	-1.92 (0.03)	(-7.2)
Last value	0.34	0.34
Mean value	0.0	0.0

248 by the GP method, is close to the R^2 -score of 0.76 which is obtained from using
 249 one Landsat observation to predict another Landsat observation of the same
 250 pixel on the same day (see Section 3). For interpolation the linear method was
 251 also somewhat effective, achieving an R^2 -score of 0.53. When SG smoothing
 252 was applied (windows of length 7 and a polynomial of order 2) after the linear
 253 interpolation, the R^2 -score rose to 0.60, which was not quite as high as that
 254 obtained from the GP method. When doing (forecast mode) extrapolation the
 255 alternatives to the GP method did not work at all (R^2 -scores were negative).

256 For the MODIS data, GP, linear interpolation and quadratic interpolation
 257 all performed similarly well. Quadratic interpolation had the highest R^2 -score,
 258 hence this method was chosen for gap-filling on the MODIS data. The higher in-
 259 terpolation R^2 -scores for MODIS, compared to Landsat, imply that the MODIS
 260 data is less noisy than the Landsat data. Assuming that observations from
 261 MODIS and Landsat have similar signal-to-noise ratio, this can be explained
 262 by the higher temporal resolution of MODIS, and the compositing of 7 daily
 263 observations for the weekly gridded MODIS data.

Table 2: R^2 -scores for different interpolation methods on the MODIS data. The interpolation score column is the mean R^2 -score for all sampled (1200) time series.

Method	Interpolation Score
GP	0.92
Linear	0.93
Quadratic	0.94
Cubic	0.92
Last value	0.70
Mean value	-0.02

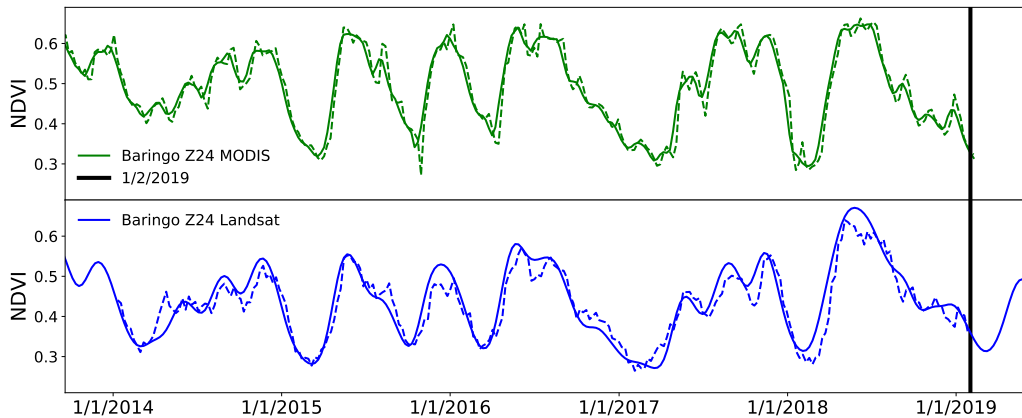


Figure 2: NDVI times series of pixels randomly selected from the intersection of Baringo county and livelihood zone 24 and aggregated. The top panel shows MODIS data, and the bottom panel shows Landsat data (solid lines), processed using the methods described in the text. The dotted lines in each panel show forecasting at a lead time of 2 weeks, using the AR method on the MODIS data, and the GP method on the Landsat data.

264 4.2. Forecasted indices and aggregation

The indices we forecasted were NDVI anomaly and VCI3M. NDVI anomaly is the mean-subtracted NDVI, where the mean is the average NDVI for the given week of the year over all years covered by the data. VCI3M is the mean VCI across the 3 months leading up to the given observation time point, with VCI at time point i being defined as

$$VCI_i = 100 \times \frac{NDVI_i - NDVI_{min,i}}{NDVI_{max,i} - NDVI_{min,i}}, \quad (6)$$

265 where $NDVI_{min,i}$ and $NDVI_{max,i}$ are the minimum and maximum values for the
266 NDVI of the pixel in the given week over all years covered by the data. Time
267 series for each of these indices were derived from the processed NDVI time
268 series. On Landsat pixels, the mean, maximum and minimum value for the
269 NDVI for each week of the year was computed using the non-forecast mode GP
270 interpolated time series. Then forecast mode and non-forecast mode versions
271 of each index were created. For forecast mode, a straight RBF kernel was used
272 with no periodic component, since seasonal periodicity is not present in NDVI
273 anomaly and VCI3M.

274 With both the Landsat and MODIS datasets, individual pixel time series for
275 each index were aggregated, by taking the mean, within each livelihood zone
276 and county intersection. Thus forecasting was carried out on a single time series
277 for each region (see Fig. 2 for an example time series). With the MODIS data,
278 since not all gaps were interpolated (see Section 4.5.2), whenever there were
279 fewer than 25 individual pixel readings from a particular region at a given time
280 point, it was decided that there should be no datum in the aggregate time series,
281 i.e. there should be a gap.⁷

⁷VCI3M is the mean of the most recent 12 weeks of VCI observations; if some of these were missing, the mean was taken over just the ones that were present. If the current observation

Table 3: Table comparing Landsat and MODIS products

Feature	Landsat	MODIS
Spatial Resolution	High resolution at 30 m	Medium resolution ranging from 250 m to 1 km
Temporal Resolution	16-day sampling (8-day when both Landsat-7 and 8 are used)	Daily sampling monitoring dynamic variables
Quality	Cloud coverage at 30 m	Cloud coverage at 500 m

²⁸² 4.3. Comparison of the two datasets

²⁸³ The key differences between the two datasets are the spatial and temporal
²⁸⁴ resolutions, see Table 3. The Landsat data had higher spatial resolution, whilst
²⁸⁵ the MODIS data had higher temporal resolution. Since forecasting was being
²⁸⁶ attempted at the level of large scale regions (livelihood zone and county inter-
²⁸⁷ sections), and at a weekly temporal resolution, the expectation was that the
²⁸⁸ MODIS data would have advantages, assuming individual Landsat and MODIS
²⁸⁹ observations have similar signal-to-noise ratios. The processed MODIS time
²⁹⁰ series with weekly datapoints have less measurement noise because they are
²⁹¹ composites of 7 daily observations, whereas the processed Landsat time series
²⁹² are derived from more temporally sparse data (up to 3 different Landsat mis-
²⁹³ sions, each yielding one observation every 16 days). Landsat data would have
²⁹⁴ advantages in different applications where forecasts on smaller spatial scales are
²⁹⁵ required. The Landsat data also has the advantage that the quality flags and
²⁹⁶ cloud masks are defined on smaller scales.

²⁹⁷ The differences between the MODIS and Landsat datasets produced slightly
²⁹⁸ different True aggregate time series on which to assess the interpolation and
²⁹⁹ forecasting methods. In addition to the different temporal resolution of the
³⁰⁰ observations supplying the final time series, the MODIS data were aggregated
³⁰¹ across 100 random grassland pixels from each region, whereas the 1 000 Land-
³⁰² sat pixels analysed were randomly distributed over the whole of each region.

was not present, a gap was placed in the VCI3M time series.

303 The MODIS grassland classification was not available at Landsat resolution,
304 thus unambiguous classification of the smaller Landsat pixels was not possible.
305 This is unlikely to have made much difference to pixel selection, given that the
306 pastoral livelihood zones are mostly grasslands (Fig. 1).

307 The ultimate test for the forecasts would be comparison with a reliable
308 ground truth. In this paper the focus is restricted to the forecasting of NDVI and
309 VCI as seen from different remote sensing observations. The MODIS predictions
310 are compared with future MODIS observations, and the Landsat predictions are
311 compared with future Landsat data.

312 *4.4. Metrics for assessing forecasts*

Several metrics were used to assess the performance of the forecast methods tested on the data. The R^2 -score and the percentage of standard deviation remaining, S , were used. These are given by:

$$R^2\text{-score} = 1 - \frac{\sum_i (y_i - f_i)^2}{\sum_i (y_i - \bar{y})^2}, \quad (7)$$

$$S = 100 \times \frac{\sqrt{\sum_i (y_i - f_i)^2}}{\sqrt{\sum_i (y_i - \bar{y})^2}}, \quad (8)$$

313 where the y_i are the true data, and the f_i are the forecasts. Note that these are
314 not independent measures and, in fact, $S \equiv 100 \times \sqrt{1 - R^2\text{-score}}$. Probability
315 distributions were also obtained for true values given forecasted values. Finally
316 receiver operating characteristic (ROC) curves were constructed for forecast-
317 based drought-alert detection, with drought-alert defined by $VCI3M < 35$.

318 4.5. Forecasting methods

319 4.5.1. GP for forecasting

320 GP forecasting on the Landsat data was tested by comparing the forecast
321 mode and non-forecast mode time series from 1/1/2014 to 1/2/2019.⁸ This
322 range for testing gave the GP sufficient time to train (1/1/2000 to 31/12/2013),
323 and is also the period for which Landsat-8 has been operational. The forecast
324 mode GP was run with different lengths of data removed; in each case the future
325 data were removed, and then data were further removed from the past 1 to 10
326 weeks to respectively assess forecasting at 1 to 10 weeks ahead. Fig. 3 shows
327 that the same approximately linear relation between NDVI anomaly and lagged
328 NDVI anomaly holds for the forecast and non-forecast mode time-series, and
329 hence gives some validation of the method.⁹

330 For the MODIS data, forecasting was performed between 1/1/2004 and
331 1/2/2019 by removing all future data (and also removing the data from the
332 past 1 to 10 weeks), creating a forecast mode GP and comparing the resulting
333 forecast observations with the corresponding removed observations.¹⁰

334 4.5.2. Linear autoregressive forecasting

The potential of forecasting via linear autoregression (AR) was assessed on the MODIS data. For forecasting n weeks ahead, the following model was fit:

$$X_{t+n} = \sum_{i=0}^{p-1} a_i X_{t-i} + \epsilon_t, \quad (9)$$

⁸Note that the forecast mode has a shorter temporal length (less training data) than for estimates of the near future in 2019. This comparison therefore provides a (small) underestimate of the quality of the predictions.

⁹The assumption, under GP interpolation and extrapolation, that data anomalies follow a multivariate Gaussian distribution necessarily also assumes that the relationship between past and present anomalies are linear. This follows from the fact that a stationary Gaussian AR process must be linear (Barrett et al., 2010).

¹⁰The forecast was only made for the dates for which AR forecasting was attempted (see Section 4.5.2 for description of exclusions).

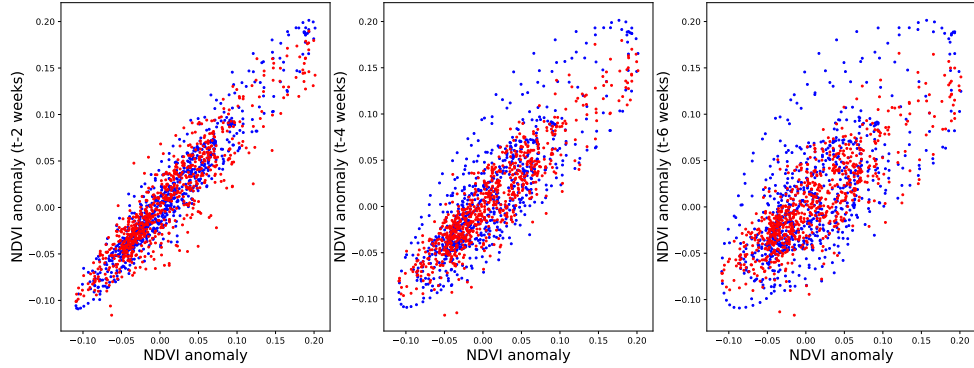


Figure 3: The approximately linear relation between Landsat NDVI anomaly and NDVI anomaly lagging at two, four and six weeks in the past. Blue dots show the Landsat data, processed with non-forecast mode GPs, which was taken as ‘ground truth’. Red dots show the data processed with forecast mode GPs, from which forecasts were generated.

335 where X is NDVI anomaly (or VCI3M with mean removed), subscripts denote
 336 the observation (week), a_i are model parameters, ϵ_t are the residuals (i.e. the
 337 errors), and p is the model order. Plots of NDVI anomaly against lagged NDVI
 338 anomaly showed that there is a strong linear relation between present and past
 339 observations of NDVI anomaly, see Fig. 3, thus it is anticipated that the linear
 340 AR model captures a good degree of the non-random relationship between past
 341 and future NDVI anomaly observations. Fitting the model to a segment of
 342 data involved finding the model parameters that gave the minimum sum-square
 343 error, i.e. led to residuals with the minimum variance. To make a forecast,
 344 the model was fit using the most recent T consecutive observations, and then
 345 used to predict the observation n weeks after the most recent observation. This
 346 forecasting method was carried out along the entire available time series, fitting
 347 a distinct model to each segment of length T . A search for optimal model orders
 348 and training segment lengths found that forecast quality, as measured by root
 349 mean square prediction error, plateaued at $T = 200$ and $p = 3$. High values of
 350 p up to 20 were explored with LASSO regression (a regularisation procedure),

351 but this led to inferior forecasting.

352 Due to the presence of some non-interpolated gaps in the MODIS time se-
353 ries, there were weeks when a forecast assessment was not carried out. For a
354 forecast assessment to be carried out: (i) the three most recent weekly aggre-
355 gated observations had to be present, so a prediction could be made; (ii) there
356 had to be an aggregated observation present for the week being forecast, so the
357 quality of the prediction could be assessed.

358 To check that results were not strongly dependent on the choice of maximum
359 allowed interpolation length L_{\max} in the gap filling (see Secion 4.1.2) the method
360 was applied to the MODIS data processed with $L_{\max} = 4$ and 8 , in addition to
361 $L_{\max} = 6$. As can be seen in Table C.5, results did not substantially depend on
362 the choice of this parameter.

363 For comparison, this method was also applied to the Landsat data. AR
364 models were fit to the forecast mode time series, and predictions from the model
365 were then compared to corresponding data on the non-forecast mode time series.

366 5. Results

367 5.1. Forecasting with GPs

368 Figure 4 shows the percentage of standard deviation remaining, S , for the
369 1-10 weeks NDVI anomaly and VCI3M forecast for the Landsat data. The
370 R^2 -score and reduction in standard deviation for the two, four and six weeks
371 forecasts for the different regions can be found in the appendix in Tables C.6 and
372 C.7 and contour plots of VCI3M forecast against actual VCI3M can be found in
373 Fig. B.10. Lower values were found for the standard deviation remaining for the
374 VCI3M than for the NDVI anomaly, which can be explained as future VCI3M
375 is an aggregate derived from past, present and future NDVI values.

376 The GP forecast method was also applied to the MODIS data, but this

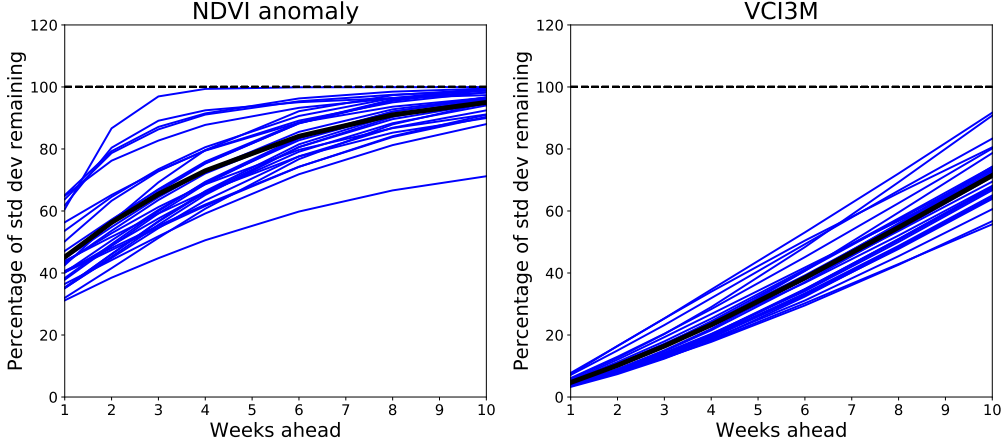


Figure 4: Forecast performance with a lead time of 1 to 10 weeks using the GP method on the Landsat data, as given by percentage standard deviation remaining S , for (Left) NDVI anomaly, and (Right) VCI3M. The blue lines show results for the individual regions (county/livelihood zone intersections), and the black line shows the median across all regions.

³⁷⁷ method was outperformed by the AR method described in Section 5.2. The
³⁷⁸ results are shown in Table C.10 in the appendix.

³⁷⁹ 5.2. Forecasting with AR modelling

³⁸⁰ The performance of the forecasting method described in Section 4.5.2 to the
³⁸¹ MODIS NDVI anomaly data are plotted in Fig. 5. Since there were gaps in the
³⁸² time series (see Section 4.5.2) a forecast assessment was not made at every time
³⁸³ point. Table C.8 in the appendix shows, for a lead time of 4 weeks, the quantity
³⁸⁴ of forecast assessments that were carried out for each region, as a percentage of
³⁸⁵ the total that would have been possible if there had been no gaps in the data.
³⁸⁶ For 15 of the regions, a forecast could be made on more than 90 percent of
³⁸⁷ weeks. However, for some of the more cloudy/wet regions we were rarely able
³⁸⁸ to make a forecast.

³⁸⁹ The linear AR method was also tested on the Landsat data, but there the
³⁹⁰ method performed less well than the GPs method. The results are shown in

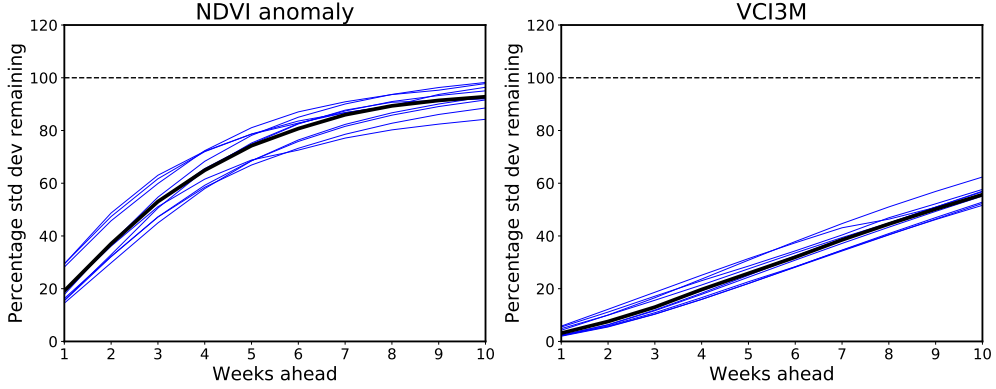


Figure 5: Forecast performance with a lead time of 1 to 10 weeks using the AR method on the MODIS data, as given by percentage standard deviation remaining, for (Left) NDVI anomaly, and (Right) VCI3M. The blue lines show results for the individual regions for which a forecast is possible more than 50% of the time, and the black line shows the median across all 19 of these regions.

³⁹¹ Table C.11 in the appendix.

³⁹² 5.2.1. Assessing forecasting with the inclusion of additional variables

For the MODIS data, we tested to see whether we could improve the prediction of NDVI anomaly by including the past of other available variables in the AR model, i.e. we performed a Granger causality analysis. Taking X as NDVI anomaly, as in equation (9), for another variable Y , the extended model was fit:

$$X_{t+n} = \sum_{i=0}^{p-1} a_i X_{t-i} + \sum_{i=0}^{q-1} b_i Y_{t-i} + \epsilon'_t, \quad (10)$$

³⁹³ and Granger causality measured as ΔR^2 , the R^2 -score obtained from this ex-
³⁹⁴ tended model minus the R^2 -score obtained from the previous (reduced) model
³⁹⁵ (9).

³⁹⁶ Firstly, we tested whether including past observations of either the red band
³⁹⁷ or the NIR band (at the same lags as NDVI anomaly) in the regression to
³⁹⁸ predict NDVI anomaly could improve the quality of the forecast, and found it
³⁹⁹ did not. For a lead time of 4 weeks, for example, the improvement in R^2 -score

400 was generally negative; the mean improvement across regions was -0.007 for red
401 and -0.01 for NIR.

402 Secondly, we tested for Granger causality of NDVI anomaly from each region
403 to each other region (within the set of regions for which predictions could be
404 made more than 50% of the time). That is, for each pair of distinct regions, i and
405 j , the 3 most recent observations from region j were added to the AR forecast
406 model for region i , and the R^2 -score was compared with that obtained without
407 including observations from region j . There was not strong Granger causality
408 of NDVI anomaly between most regions. For only a few combinations was there
409 an improvement in R^2 -score of more than 0.05, see Fig. 6. Nevertheless, these
410 results suggest that, to create the optimal linear regression based forecasting
411 method, data from all regions should be used. Future work will explore how
412 best to extract any useful information from regions other than the one being
413 forecast.

414 5.3. Drought event forecast: ROC curves

415 To assess the usefulness of the AR and GP methods for drought forecasting,
416 we tested their ability to detect specific drought events, as defined by the
417 NDMA's alert threshold ($VCI3M < 35$, Klisch and Atzberger, 2016). Receiver
418 operating characteristic (ROC) curves were plotted for detection of $VCI3M < 35$
419 at lead times of two, four and six weeks (Fig. 7). These curves show the probability
420 of predicting a state of drought ($VCI3M < 35$) when there will be a state of
421 drought, i.e. hit rate, against the probability of predicting drought when there
422 will not be drought, i.e. false alarm rate, for varying binarisation thresholds on
423 the forecast. These curves give an indication that one can forecast droughts
424 with these methods even as far as six weeks ahead.

425 The ROC curve performance is not highly dependent on the region (see Table 4). Even for the wetter Eastern regions, for which observations are sparser

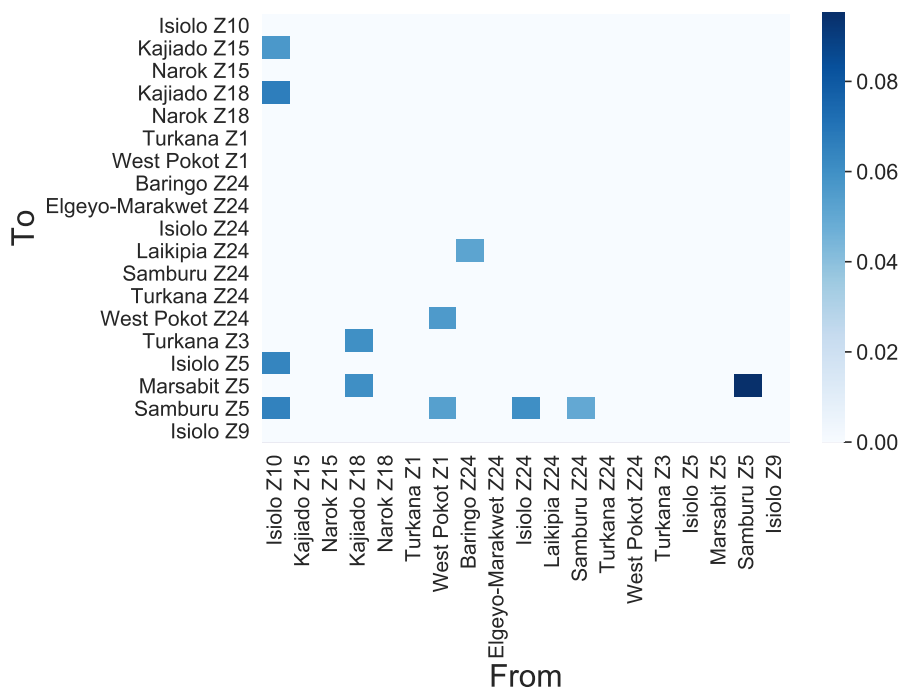


Figure 6: Granger causality of NDVI anomaly from each region to each other region, computed on the MODIS data, measured as improvement in R^2 -score when observations from region ‘From’ are added to the AR model for forecasting region ‘To’ at a lead time of 4 weeks. Only substantial Granger causalities are shown, i.e. those with $\Delta R^2 > 0.05$.

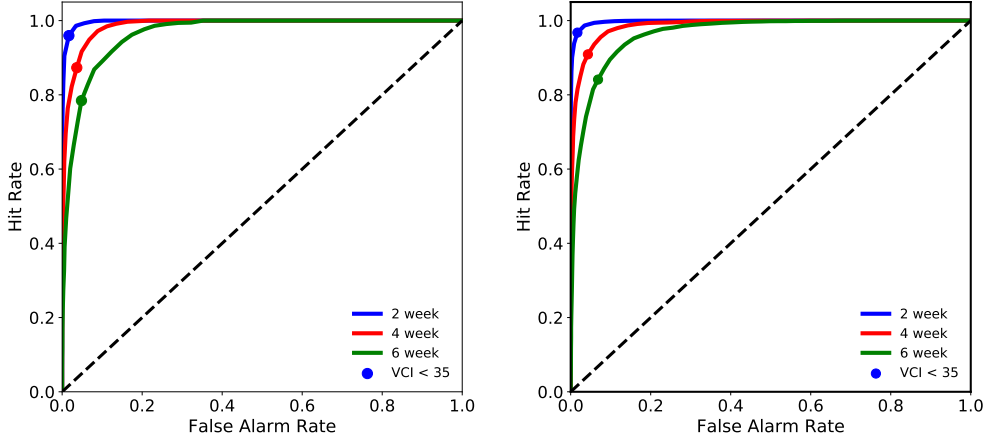


Figure 7: (Left) ROC curve for drought detection ($VCI_{3M} < 35$) for lead times of 2, 4 and 6 weeks using the GP method. (Right) ROC curve for drought detection using the AR method. The curves are plotted from applying different thresholds to convert the continuous forecast into a binary forecast of drought or no drought, see text for details. The shaded circles show the point obtained from forecasting drought when the predicted $VCI_{3M} < 35$. The area under the curve is 1.0, 0.98, 0.96 (GP, left) and 1.0, 0.99 and 0.96 (AR, right) for lead times of two, four and six weeks, respectively.

due to cloud cover, the hit and false alarm rates only differ by 1 to 2 percentage points compared with those computed across all regions. Together, these results demonstrate that there is a huge potential for drought forecasting, and encourage a future cost-benefit analysis of applying such a forecast in practice.

Table 4: False alarm rate and hit rate (respectively, in percent) for different regions in Kenya based on forecasting drought if the predicted VCI_{3M} is less than 35.

Regions	Landsat GP						MODIS AR					
	2 weeks		4 weeks		6 weeks		2 weeks		4 weeks		6 weeks	
All	2%	96%	4%	87%	5%	78%	2%	97%	4%	91%	7%	84%
Z24	2%	99%	4%	91%	5%	82%	2%	98%	5%	94%	8%	88%
North (Z1,3 and 5)	1%	97%	2%	88%	3%	76%	2%	98%	6%	93%	11%	87%
East (Z7, 9, 10 and 11)	3%	94%	5%	85%	6%	77%	3%	97%	6%	91%	10%	85%
South (Z15 and 18)	1%	96%	3%	88%	4%	77%	2%	98%	6%	94%	11%	90%

431 **6. Discussion and Conclusion**

432 This paper highlights the potential of two separate methods for drought fore-
433 casting in pastoral regions of Kenya. The linear autoregression models applied
434 to MODIS achieved an R^2 -score of 0.58 for NDVI anomaly at a lead time of
435 4 weeks, and an R^2 -score of 0.95 for the VCI3M, the three-month vegetation
436 condition index used within the drought early warning system developed by
437 the National Drought Management Authority. The Gaussian Processes method
438 was applied to Landsat and achieved an R^2 -score of 0.36 for NDVI anomaly at
439 a lead time of 4 weeks, and an R^2 -score of 0.94 for the VCI3M. Importantly,
440 both methods showed high sensitivity and specificity for prediction of VCI val-
441 ues indicative of drought, at lead times of 2, 4 and 6 weeks (see Fig. 7). We
442 have presented results at the level of livelihood zone and county intersections,
443 however both methods can be applied at any suitable spatial unit (e.g., grazing
444 units) due to the high spatial resolution of both satellite datasets.

445 Both methods constitute novel analyses of vegetation index time series. To
446 our knowledge, this is the first time that the GP method for NDVI forecasting
447 has been applied to large amounts of real data and used for gap-filling. We
448 have shown that GPs are a very useful addition to other methods for both these
449 purposes. Similarly, linear AR of NDVI, or of Granger causality of various
450 variables to NDVI, has not previously been explored at a temporal resolution
451 as fine as 1 week. That such substantial R^2 -scores can be achieved for NDVI
452 anomaly at a lead-time of several weeks just by using the past few observations
453 of NDVI anomaly in a linear AR model is a novel finding. Furthermore we
454 moved beyond fitting a single model, and rather fit models to segments of data,
455 repeatedly using refreshed models to forecast subsequent observations not used
456 in the model fitting (i.e. we had separation of training and testing models).

457 Droughts have many adverse effects on pastoral and agro-pastoral commu-

nities as they mainly rely on rainfall for food and fodder availability. In order to reduce drought-related damage and losses within these communities, local, national, and international stakeholders often decide to act on information provided by EWS which may come too late (Kim and Guha-Sapir, 2012). Indeed, these systems tend to monitor current, rather than forecast future, environmental and socio-economic factors in a region, and sound the alarm when the situation is already critical. Some EWS now include a qualitative assessment of future rainfall. However, a meteorological or hydrological drought will not necessarily lead to agricultural damage (Bhuiyan et al., 2006). To mitigate the impacts on food security and nutrition, EWS need to focus on monitoring and forecasting the possible socio-economic impacts of future rainfall variability on agricultural drought (WMO, 2015). Additionally, acting ahead of a disaster instead of providing humanitarian assistance once a disaster hits can save money and lives (Venton et al., 2012). The methods developed in this study allow disaster risk managers to estimate vegetation condition to access resources and limit the impacts for pastoralist communities up to six weeks ahead. For example, in Kenya, the emergency funds that are linked to the VCI could be accessed earlier to launch livestock destocking and vaccination campaigns. Future work should focus on methods that forecast socio-economic drought indicators such as livestock mortality, milk production, or food prices.

Droughts are complex and hence inherently difficult to define and measure (Mishra and Singh, 2010). A large number of satellite-based indicators have been developed to identify meteorological, hydrological, and agricultural droughts (Zargar et al., 2011; AghaKouchak et al., 2015) with each performing well in space and time to a certain degree (Zhang et al., 2017). While its limitations are known, the VCI used in this study has been introduced as one of the main biophysical indicators in the drought early warning system operated by the

485 NDMA, with specific thresholds to identify different levels of drought throughout
486 the ASAL regions of Kenya (Klisch and Atzberger, 2016). In future, we suggest
487 that the performance of this indicator together with the thresholds used should
488 be linked to ground-based measurements over various agro-ecological zones.

489 Droughts have devastating impacts on many people around the world. There
490 are increasing efforts to develop tools and identify actions to save lives and
491 livelihoods before these disasters strike. The methods developed in this study
492 can help policy makers, disaster risk managers and other key stakeholders to
493 understand up to six weeks in advance the state of vegetation in pastoralist
494 areas. This will allow them to access resources and develop procedures before
495 the impacts of drought become visible to mitigate the adverse effects in these
496 vulnerable communities. To further strengthen EWS, future research needs to
497 clearly identify satellite-based indicators and thresholds of drought (which may
498 vary in time and space), to build a relation between observable indices and
499 future impacts. More work is also needed to understand how a hazard (e.g.,
500 reduced rainfall) becomes a disaster (e.g., food insecurity) so that these events
501 can be better forecasted.

502 **Authors responsibilities**

503 A.B.B., S.D. and E.S. are lead authors as they contributed equally to the
504 paper and the order of the three names is alphabetical. A.B.B was responsible
505 for the Linear AR and Granger causality calculations, and the text describing
506 those methods. S.D. was responsible for the GPs used in the paper and was
507 responsible for the usage of all the Landsat data and the text describing those
508 methods. E.S. was responsible for the MODIS data accumulation, creation of
509 the MODIS time series and the filtering of the MODIS data and the text describ-
510 ing those methods. SO and PR developed the initial idea and provided feedback

511 throughout. All authors wrote, reviewed and edited the final manuscript. We
512 acknowledge early contributions to pilot work from Peter Hurley, Philip Rooney,
513 Martin Jung, and Jörn Scharlemann.

514 **Acknowledgements**

515 This research was funded by the STFC through the following projects: “As-
516 troCast: Applying Astronomy Data Analysis to enhance disaster forecasting”
517 – grant number ST/R004811/1; and “STFC Official Development Assistance
518 (ODA) Institutional Award” attached to the same grant and; ”A UK-Africa
519 Data Science Network: Capturing the SKA-Driven Data Transformation” grant
520 number ST/R001898/1. This project was initiated through pump-priming fund-
521 ing from the University of Sussex’s “Sussex Research” thematic programme and
522 carried out as part of the interdisciplinary Data Intensive Science Centre at the
523 University of Sussex (DISCUS)

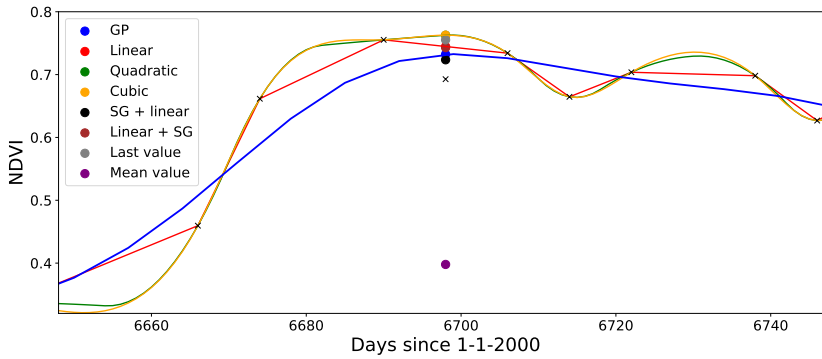


Figure A.8: An example of our interpolation method on a Landsat pixel, the black crosses show the real data, where the datum at day 6698 is removed. The colored dots show our interpolated value at day 6698 using the different methods. The blue, red, green and yellow lines show the complete interpolation for every date.

524 **Appendix A. Interpolation**

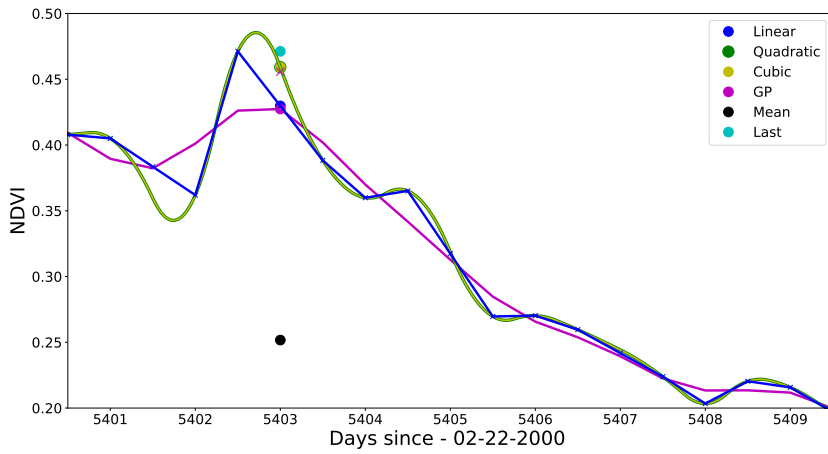


Figure A.9: An example of our interpolation method on MODIS pixels, the blue cross point show the point at day 5403, where the datum was dropped. The colored dots show our interpolated values using the different methods.

525 **Appendix B. Forecast**

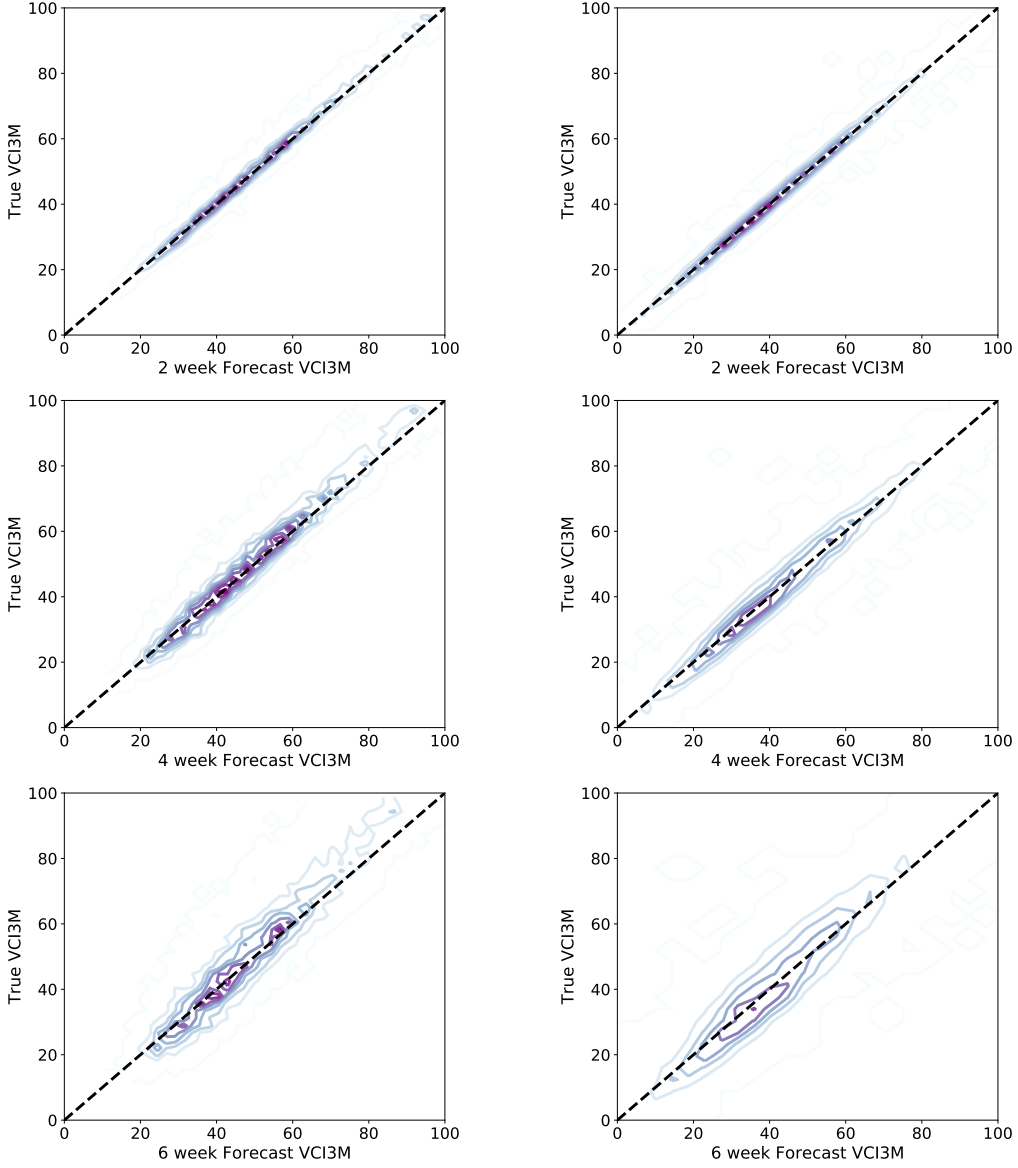


Figure B.10: Contour plots of VCI3M against our two, four and six weeks VCI3m forecast. The left three plots show our forecast performance for the GP method on Landsat data, and on the right the contours show the forecast performance for the AR method on MODIS data.

Table C.5: Comparison of outcomes for different choices of maximum allowed interpolation length L_{\max} on the MODIS data. Percentage standard deviation remaining, S , at 4 weeks, and the percentage of the time that it was possible to make a forecast (non-interpolated gaps lead to it not being possible to make a forecast every week, see main text for details), for $L_{\max} = 4, 6$, and 8 . Numbers show the median across all regions.

L_{\max}	S at 4 weeks	Forecasts attempted (%)
4	63	84
6	65	93
8	61	98

526 **Appendix C. Tables of NDVI and VCI3M forecast**

Table C.6: NDVI anomaly forecast using Landsat data for the 29 regions. The numbers shown are the proportion of standard deviation remaining (Equation 8) and the R^2 -score for NDVI anomaly. We only used past data for the interpolation and we the average value for every pixel within the region for the region estimate. The * indicates regions where a minimum of 180 detections per pixel were used, instead of 250.

Region	2 weeks	4 weeks	6 weeks
Baringo Z24	46 0.74	66 0.46	81 0.19
Elgeyo-Marakwet Z24	49 0.74	69 0.47	83 0.22
Garissa Z10*	55 0.64	73 0.36	86 0.12
Garissa Z11*	63 0.58	80 0.33	89 0.16
Isiolo Z5	57 0.64	75 0.37	88 0.13
Isiolo Z9	65 0.53	79 0.30	89 0.13
Isiolo Z10	79 0.31	91 0.08	96 -0.02
Isiolo Z24	57 0.67	76 0.41	89 0.19
Kajiado Z15	45 0.76	63 0.52	78 0.28
Kajiado Z18*	44 0.75	59 0.55	72 0.34
Laikipia Z24	42 0.82	61 0.62	77 0.39
Lamu Z11*	80 0.33	92 0.12	95 0.07
Mandera Z7	76 0.25	88 0.00	93 -0.13
Mandera Z9	53 0.44	69 0.06	80 -0.27
Marsabit Z5	52 0.60	66 0.35	78 0.11
Marsabit Z7*	47 0.76	62 0.59	74 0.40
Narok Z15	56 0.67	80 0.34	92 0.12
Narok Z18	56 0.68	75 0.42	88 0.20
Samburu Z5	49 0.68	69 0.36	84 0.08
Samburu Z24	45 0.78	65 0.54	81 0.30
Tana River Z11*	65 0.57	81 0.33	91 0.15
Turkana Z1	54 0.56	72 0.21	84 -0.09
Turkana Z3	38 0.61	51 0.33	60 0.06
Turkana Z24	46 0.75	66 0.48	81 0.21
Wajir Z7*	48 0.71	62 0.51	74 0.30
Wajir Z9	79 0.20	91 -0.07	95 -0.18
Wajir Z10	87 0.24	99 0.01	100 0.00
WestPokot Z1	50 0.69	69 0.43	83 0.18
WestPokot Z24	49 0.68	66 0.42	79 0.16
Median	53 0.67	69 0.36	84 0.15

Table C.7: VCI3M forecast performance using GPs on the Landsat data. The numbers shown are the percentage standard deviation remaining and the R^2 score, respectively.

Region	2 weeks	4 weeks	6 weeks
Baringo Z24	9 0.99	22 0.95	38 0.86
Elgeyo-Marakwet Z24	9 0.99	21 0.96	36 0.87
Garissa Z10	10 0.99	23 0.95	39 0.85
Garissa Z11	11 0.99	25 0.94	41 0.83
Isiolo Z5	10 0.99	23 0.95	39 0.85
Isiolo Z9	11 0.99	24 0.94	38 0.85
Isiolo Z10	13 0.98	29 0.92	46 0.79
Isiolo Z24	10 0.99	23 0.95	39 0.85
Kajiado Z15	9 0.99	21 0.96	36 0.87
Kajiado Z18	9 0.99	20 0.96	34 0.88
Laikipia Z24	7 0.99	18 0.97	32 0.89
Lamu Z11	13 0.98	29 0.92	45 0.80
Mandera Z7	15 0.98	32 0.90	49 0.76
Mandera Z9	12 0.98	29 0.92	48 0.77
Marsabit Z5	11 0.99	25 0.94	41 0.83
Marsabit Z7	8 0.99	19 0.96	32 0.90
Narok Z15	10 0.99	25 0.94	41 0.83
Narok Z18	11 0.99	24 0.94	40 0.84
Samburu Z5	10 0.99	24 0.94	42 0.83
Samburu Z24	8 0.99	20 0.96	35 0.88
TanaRiver Z11	11 0.99	24 0.94	40 0.84
Turkana Z1	14 0.98	31 0.90	52 0.73
Turkana Z3	12 0.99	26 0.93	43 0.81
Turkana Z24	9 0.99	22 0.95	38 0.85
Wajir Z7	9 0.99	20 0.96	34 0.88
Wajir Z9	16 0.97	35 0.88	53 0.72
Wajir Z10	17 0.97	35 0.88	52 0.73
WestPokot Z1	9 0.99	23 0.95	39 0.85
WestPokot Z24	10 0.99	22 0.95	38 0.85
Median	10 0.99	24 0.94	39 0.85

Table C.8: VCI3M forecast performance using AR on the MODIS data. The numbers shown are the percentage standard deviation remaining and the R^2 score, respectively. In the 'Forecasts' column, the number gives the percentage of time points for which it was possible to obtain a forecast (long gaps in the data sometimes impaired the ability to produce a forecast, see Sec. 4.5.2 for details).

Region	2 weeks	4 weeks	6 weeks	Forecasts
Baringo Z24	6 0.99	18 0.96	32 0.89	100
Elgeyo-Marakwet Z24	6 0.99	18 0.96	32 0.89	95
Garissa Z10	11 0.98	20 0.95	53 0.71	15
Garissa Z11	xx xx	xx xx	xx xx	0
Isiolo Z5	12 0.98	27 0.92	42 0.81	97
Isiolo Z9	13 0.98	28 0.91	43 0.81	89
Isiolo Z10	13 0.98	28 0.91	42 0.81	71
Isiolo Z24	8 0.99	22 0.95	37 0.86	93
Kajiado Z15	12 0.98	26 0.92	39 0.84	75
Kajiado Z18	11 0.98	24 0.94	38 0.85	71
Laikipia Z24	9 0.99	23 0.94	37 0.85	93
Lamu Z11	xx xx	xx xx	xx xx	0
Mandera Z7	15 0.97	34 0.87	53 0.71	44
Mandera Z9	16 0.97	35 0.87	55 0.69	43
Marsabit Z5	9 0.99	21 0.95	34 0.88	94
Marsabit Z7	17 0.96	35 0.87	48 0.76	34
Narok Z15	11 0.98	28 0.92	44 0.79	96
Narok Z18	6 0.99	19 0.96	32 0.89	98
Samburu Z24	5 0.99	16 0.97	30 0.90	100
Samburu Z5	7 0.99	21 0.95	37 0.86	100
Tana River Z11	11 0.98	22 0.95	33 0.88	41
Turkana Z1	7 0.99	20 0.95	35 0.87	98
Turkana Z3	7 0.99	23 0.94	40 0.83	100
Turkana Z24	7 0.99	20 0.95	35 0.87	100
Wajir Z7	14 0.97	30 0.90	44 0.79	45
Wajir Z9	16 0.97	33 0.88	50 0.74	41
Wajir Z10	12 0.98	23 0.94	33 0.88	19
West Pokot Z1	7 0.99	21 0.95	38 0.85	100
West Pokot Z24	9 0.99	22 0.94	36 0.86	94
Median	11 0.99	23 0.95	38 0.85	93

Table C.9: NDVI anomaly forecast performance using AR on the MODIS data. The numbers shown are the percentage standard deviation remaining and the R^2 score, respectively.

Region	2 weeks	4 weeks	6 weeks
Baringo Z24	32 0.90	59 0.65	75 0.42
Elgeyo-Marakwet Z24	32 0.90	58 0.66	73 0.46
Garissa Z10	42 0.82	51 0.74	56 0.68
Garissa Z11	xx xx	xx xx	xx xx
Isiolo Z5	55 0.69	79 0.37	90 0.18
Isiolo Z9	36 0.87	64 0.58	80 0.35
Isiolo Z10	37 0.86	65 0.57	82 0.32
Isiolo Z24	29 0.91	57 0.66	76 0.42
Kajiado Z15	47 0.78	71 0.48	82 0.31
Kajiado Z18	45 0.79	72 0.48	87 0.24
Laikipia Z24	38 0.85	62 0.60	77 0.40
Lamu Z11	xx xx	xx xx	xx xx
Mandera Z7	33 0.89	64 0.58	87 0.24
Mandera Z9	32 0.89	65 0.57	90 0.18
Marsabit Z5	38 0.85	64 0.59	75 0.44
Marsabit Z7	35 0.88	58 0.66	71 0.49
Narok Z15	48 0.76	72 0.48	83 0.30
Narok Z18	36 0.87	61 0.62	72 0.47
Samburu Z24	28 0.92	56 0.68	73 0.46
Samburu Z5	47 0.78	74 0.45	86 0.25
Tana River Z11	53 0.71	68 0.54	87 0.24
Turkana Z1	32 0.89	64 0.58	82 0.32
Turkana Z3	33 0.89	71 0.49	88 0.21
Turkana Z24	31 0.90	62 0.61	80 0.35
Wajir Z7	29 0.91	54 0.70	67 0.54
Wajir Z9	30 0.91	57 0.67	74 0.44
Wajir Z10	26 0.93	37 0.86	46 0.79
West Pokot Z1	37 0.86	68 0.53	85 0.28
West Pokot Z24	42 0.82	65 0.57	78 0.39
Median	36 0.87	65 0.58	80 0.35

Table C.10: NDVI anomaly forecast performance using GPs on the MODIS data. The numbers shown are the percentage standard deviation remaining and the R^2 score, respectively.

Region	2 weeks	4 weeks	6 weeks
Baringo Z24	37 0.86	73 0.44	93 0.10
Elgeyo-Marakwet Z24	37 0.85	73 0.40	91 0.07
Garissa Z10	46 0.75	59 0.50	68 0.21
Garissa Z11	xx xx	xx xx	xx xx
Isiolo Z5	60 0.60	87 0.16	96 0.02
Isiolo Z9	42 0.83	79 0.38	97 0.08
Isiolo Z10	41 0.82	77 0.36	95 0.05
Isiolo Z24	34 0.89	70 0.51	92 0.15
Kajiado Z15	48 0.75	76 0.35	90 0.09
Kajiado Z18	47 0.78	77 0.40	94 0.11
Laikipia Z24	43 0.81	72 0.46	89 0.16
Lamu Z11	xx xx	xx xx	xx xx
Mandera Z7	39 0.86	74 0.50	97 0.17
Mandera Z9	35 0.89	71 0.54	96 0.20
Marsabit Z5	42 0.79	69 0.37	80 0.11
Marsabit Z7	37 0.80	61 0.38	74 0.09
Narok Z15	50 0.72	76 0.32	87 0.09
Narok Z18	39 0.84	74 0.42	90 0.11
Samburu Z5	50 0.70	80 0.26	91 0.05
Samburu Z24	34 0.88	71 0.48	92 0.12
TanaRiver Z11	60 0.47	75 0.13	87 -0.00
Turkana Z1	36 0.87	75 0.44	95 0.10
Turkana Z3	35 0.88	80 0.37	99 0.03
Turkana Z24	35 0.87	75 0.42	95 0.07
Wajir Z7	31 0.86	57 0.45	72 0.15
Wajir Z9	36 0.85	65 0.45	79 0.15
Wajir Z10	37 0.77	53 0.37	68 -0.17
WestPokot Z1	41 0.83	77 0.39	96 0.08
WestPokot Z24	49 0.78	86 0.34	103 0.06
Median	39 0.83	74 0.40	92 0.09

Table C.11: NDVI anomaly forecast performance using AR on Landsat data. The numbers shown are the percentage standard deviation remaining and the R^2 score, respectively.

Region	2 weeks	4 weeks	6 weeks
Baringo Z24	67 0.54	89 0.19	105 -0.12
Elgeyo-Marakwet Z24	74 0.44	98 0.03	113 -0.28
Garissa Z10	77 0.39	96 0.07	108 -0.17
Garissa Z11	78 0.38	94 0.10	106 -0.13
Isiolo Z5	86 0.25	103 -0.06	114 -0.31
Isiolo Z9	96 0.06	109 -0.20	116 -0.35
Isiolo Z10	108 -0.17	120 -0.46	126 -0.60
Isiolo Z24	66 0.55	82 0.31	92 0.13
Kajiado Z15	59 0.64	78 0.38	91 0.15
Kajiado Z18	60 0.63	76 0.40	90 0.18
Laikipia Z24	54 0.70	75 0.42	93 0.12
Lamu Z11	88 0.20	97 0.05	103 -0.07
Mandera Z7	78 0.38	87 0.23	93 0.12
Mandera Z9	56 0.67	69 0.51	76 0.41
Marsabit Z5	76 0.41	91 0.15	103 -0.07
Marsabit Z7	52 0.72	66 0.55	78 0.38
Narok Z15	79 0.36	101 -0.02	109 -0.19
Narok Z18	73 0.46	91 0.15	101 -0.02
Samburu Z5	74 0.44	95 0.08	110 -0.21
Samburu Z24	60 0.63	81 0.32	97 0.05
TanaRiver Z11	90 0.17	108 -0.18	120 -0.46
Turkana Z1	80 0.35	103 -0.07	118 -0.39
Turkana Z3	75 0.43	95 0.09	111 -0.24
Turkana Z24	69 0.52	91 0.16	106 -0.14
Wajir Z7	53 0.70	63 0.59	70 0.50
Wajir Z9	77 0.40	85 0.27	84 0.27
Wajir Z10	100 0.00	111 -0.24	117 -0.37
WestPokot Z1	70 0.50	92 0.15	107 -0.15
WestPokot Z24	73 0.45	96 0.06	114 -0.31
Median	74 0.44	92 0.15	106 -0.13

527 **References**

- 528 AghaKouchak A, Farahmand A, Melton F, Teixeira J, Anderson M, Wardlow
529 BD, Hain C. Remote sensing of drought: Progress, challenges and opportu-
530 nities. *Reviews of Geophysics* 2015;53(2):452–80.
- 531 Asoka A, Mishra V. Prediction of vegetation anomalies to improve food
532 security and water management in india. *Geophysical Research Letters*
533 2015;42(13):5290–8. URL: <https://agupubs.onlinelibrary.wiley.com/doi/abs/10.1002/2015GL063991>. doi:10.1002/2015GL063991.
534 arXiv:<https://agupubs.onlinelibrary.wiley.com/doi/pdf/10.1002/2015GL063991>.
- 535
- 536 Barrett AB, Barnett L, Seth AK. Multivariate granger causality and generalized
537 variance. *Phys Rev E* 2010;81:041907. URL: <https://link.aps.org/doi/10.1103/PhysRevE.81.041907>. doi:10.1103/PhysRevE.81.041907.
- 538
- 539 Behnke R, Muthami D. The Contribution of Livestock to the Kenyan
540 Economy. Technical Report; 2011. URL: https://cgspace.cgiar.org/bitstream/handle/10568/24972/IGAD{_}LPI{_}WP{_}03-11.pdf?sequence=1&isAllowed=y.
- 541
- 542
- 543 Bhuiyan C, Singh R, Kogan F. Monitoring drought dynamics in the aravalli
544 region (india) using different indices based on ground and remote sensing
545 data. *International Journal of Applied Earth Observation and Geoinforma-*
546 *tion* 2006;8(4):289 – 302. URL: <http://www.sciencedirect.com/science/article/pii/S030324340600016X>. doi:<https://doi.org/10.1016/j.jag.2006.03.002>.
- 547
- 548
- 549 Brahim-Belhouari S, Vesin JM. Bayesian learning using gaussian process for
550 time series prediction. In: Proceedings of the 11th IEEE Signal Processing
551 Workshop on Statistical Signal Processing (Cat. No.01TH8563). 2001. p. 433–
552 6. doi:10.1109/SSP.2001.955315.

- 553 Brown ME, Kshirsagar V. Weather and international price shocks on food
554 prices in the developing world. Global Environmental Change 2015;35:31
555 – 40. URL: <http://www.sciencedirect.com/science/article/pii/S0959378015300248>. doi:<https://doi.org/10.1016/j.gloenvcha.2015.08.003>.
- 558 Camps-Valls G, Verrelst J, Munoz-Mari J, Laparra V, Mateo-Jimenez F, Gomez-
559 Dans J. A survey on gaussian processes for earth-observation data analysis: A
560 comprehensive investigation. IEEE Geoscience and Remote Sensing Magazine
561 2016;4(2):58–78. doi:[10.1109/MGRS.2015.2510084](https://doi.org/10.1109/MGRS.2015.2510084).
- 562 Chandola V, Vatsavai RR. A scalable gaussian process analysis algorithm
563 for biomass monitoring. Statistical Analysis and Data Mining: The ASA
564 Data Science Journal 2011;4(4):430–45. URL: <https://onlinelibrary.wiley.com/doi/abs/10.1002/sam.10129>. doi:[10.1002/sam.10129](https://doi.org/10.1002/sam.10129).
566 arXiv:<https://onlinelibrary.wiley.com/doi/pdf/10.1002/sam.10129>.
- 567 Chen J, Jönsson P, Tamura M, Gu Z, Matsushita B, Eklundh L. A simple
568 method for reconstructing a high-quality NDVI time-series data set based on
569 the Savitzky-Golay filter. Remote Sensing of Environment 2004;91(3-4):332–
570 44. doi:[10.1016/j.rse.2004.03.014](https://doi.org/10.1016/j.rse.2004.03.014).
- 571 Dandan Xu XG. Compare ndvi extracted from landsat 8 imagery with that
572 from landsat 7 imagery. American Journal of Remote Sensing 2014;2(2):10–4.
573 doi:[10.11648/j.ajrs.20140202.11](https://doi.org/10.11648/j.ajrs.20140202.11).
- 574 Duvenaud D, Lloyd J, Grosse R, Tenenbaum J, Zoubin G. Structure discov-
575 ery in nonparametric regression through compositional kernel search. In:
576 Dasgupta S, McAllester D, editors. Proceedings of the 30th International
577 Conference on Machine Learning. Atlanta, Georgia, USA: PMLR; volume 28

- 578 of *Proceedings of Machine Learning Research*; 2013. p. 1166–74. URL:
579 <http://proceedings.mlr.press/v28/duvenaud13.html>.
- 580 FAO . Food and Agriculture Organization(FAO) COUNTRY PROGRAMMING
581 FRAMEWORK FOR KENYA (2014-2017). Technical Report; 2014. URL:
582 www.fao.org/publications.
- 583 FEWS-NET . Scenario development for food security early warning.
584 2018. URL: https://fews.net/sites/default/files/documents/reports/Guidance_Document_Scenario_Development_2018.pdf.
- 586 Galvin KA, Boone RB, Smith NMS, Lynn SM. Impacts of climate variability
587 on east african pastoralists: linking social science and remote sensing. 2001..
- 588 Hamilton J. Time series analysis. Princeton, NJ: Princeton University Press,
589 1994.
- 590 Kandasamy S, Baret F, Verger A, Neveux P, Weiss M. A comparison
591 of methods for smoothing and gap filling time series of remote sensing
592 observations – application to modis lai products. Biogeosciences
593 2013;10(6):4055–71. URL: <https://www.biogeosciences.net/10/4055/2013/>. doi:10.5194/bg-10-4055-2013.
- 595 Kim JJ, Guha-Sapir D. Famines in africa: is early warning early
596 enough? Global Health Action 2012;5(1):18481. URL: <https://doi.org/10.3402/gha.v5i0.18481>.
597 doi:10.3402/gha.v5i0.18481.
598 arXiv:<https://doi.org/10.3402/gha.v5i0.18481>.
- 599 Klisch A, Atzberger C. Operational drought monitoring in kenya using modis
600 ndvi time series. Remote Sensing 2016;8(4). URL: <http://www.mdpi.com/2072-4292/8/4/267>. doi:10.3390/rs8040267.

- 602 Kogan F. Application of vegetation index and brightness temperature
603 for drought detection. Advances in Space Research 1995;15(11):91 –
604 100. URL: <http://www.sciencedirect.com/science/article/pii/027311779500079T>. doi:[https://doi.org/10.1016/0273-1177\(95\)00079-T](https://doi.org/10.1016/0273-1177(95)00079-T); natural Hazards: Monitoring and Assessment Using Remote
606 Sensing Technique.
- 608 Kogan F, Adamenko T, Guo W. Global and regional drought dynamics in the
609 climate warming era. Remote Sensing Letters 2013;4(4):364–72. URL: <https://doi.org/10.1080/2150704X.2012.736033>. doi:10.1080/2150704X.2012.736033. arXiv:<https://doi.org/10.1080/2150704X.2012.736033>.
- 612 Lesk C, Rowhani P, Ramankutty N. Influence of extreme weather disasters on
613 global crop production. Nature 2016;529:84 EP –. URL: <https://doi.org/10.1038/nature16467>.
- 615 Mishra AK, Singh VP. A review of drought concepts. Journal of Hydrology
616 2010;391(1):202 –16. URL: <http://www.sciencedirect.com/science/article/pii/S0022169410004257>. doi:<https://doi.org/10.1016/j.jhydrol.2010.07.012>.
- 619 Nelson GC, Valin H, Sands RD, Havlík P, Ahammad H, Deryng D, El-
620 liott J, Fujimori S, Hasegawa T, Heyhoe E, Kyle P, Von Lampe
621 M, Lotze-Campen H, Mason d'Croz D, van Meijl H, van der Mens-
622 brugghe D, Müller C, Popp A, Robertson R, Robinson S, Schmid E,
623 Schmitz C, Tabeau A, Willenbockel D. Climate change effects on agri-
624 culture: Economic responses to biophysical shocks. Proceedings of
625 the National Academy of Sciences 2014;111(9):3274–9. URL: <https://www.pnas.org/content/111/9/3274>. doi:10.1073/pnas.1222465110.
626 arXiv:<https://www.pnas.org/content/111/9/3274.full.pdf>.

- 628 Nyong A, Adesina F, Osman Elasha B. The value of indigenous knowledge
629 in climate change mitigation and adaptation strategies in the african sa-
630 hel. Mitigation and Adaptation Strategies for Global Change 2007;12(5):787–
631 97. URL: <https://doi.org/10.1007/s11027-007-9099-0>. doi:10.1007/
632 s11027-007-9099-0.
- 633 Orindi V, Nyong A, Herrero MT. Pastoral livelihood adaptation to drought and
634 institutional interventions in kenya 2007;.
- 635 Papagiannopoulou C, Gonzalez Miralles D, Decubber S, Demuzere M, Ver-
636 hoest N, Dorigo WA, Waegeman W. A non-linear granger-causality frame-
637 work to investigate climate-vegetation dynamics. GEOSCIENTIFIC MODEL
638 DEVELOPMENT 2017;10(5):1945–60. URL: <http://dx.doi.org/10.5194/gmd-10-1945-2017>.
- 640 Coughlan de Perez E, van den Hurk B, van Aalst MK, Jongman B,
641 Klose T, Suarez P. Forecast-based financing: an approach for cat-
642 alyzing humanitarian action based on extreme weather and climate fore-
643 casts. Natural Hazards and Earth System Sciences 2015;15(4):895–
644 904. URL: <https://www.nat-hazards-earth-syst-sci.net/15/895/2015/>. doi:10.5194/nhess-15-895-2015.
- 646 Piguet E, Poudou A, de Guchteneire P. Migration and Climate Change:
647 An Overview. Refugee Survey Quarterly 2011;30(3):1–23. URL:
648 <https://doi.org/10.1093/rsq/hdr006>. doi:10.1093/rsq/hdr006.
649 arXiv:<http://oup.prod.sis.lan/rsq/article-pdf/30/3/1/4460951/hdr006.pdf>.
- 650 Tozier de la Poterie A, Baudoin MA. From yokohama to sendai: Approaches
651 to participation in international disaster risk reduction frameworks. Inter-
652 national Journal of Disaster Risk Science 2015;6(2):128–39. URL: <https://doi.org/10.1007/s13753-015-0053-6>.

- 654 Rasmussen CE, Williams CKI. Gaussian processes for machine learning 2006;.
- 655 Rojas O, Vrieling A, Rembold F. Assessing drought probability for agri-
656 cultural areas in africa with coarse resolution remote sensing imagery.
657 Remote Sensing of Environment 2011;115(2):343 –52. URL: <http://www.sciencedirect.com/science/article/pii/S0034425710002798>.
658 doi:<https://doi.org/10.1016/j.rse.2010.09.006>.
- 660 Roy D, Wulder M, Loveland T, Woodcock C, Allen R, Anderson M, Helder D,
661 Irons J, Johnson D, Kennedy R, Scambos T, Schaaf C, Schott J, Sheng Y, Ver-
662 mote E, Belward A, Bindschadler R, Wohen W, Gao F, Zhu Z. Landsat-8: Sci-
663 ence and product vision for terrestrial global change research. Remote Sensing
664 of Environment 2014;2014:154–72. doi:[10.1016/j.rse.2014.02.001](https://doi.org/10.1016/j.rse.2014.02.001).
- 665 Rulinda CM, Bijker W, Stein A. The chlorophyll variability in meteosat derived
666 ndvi in a context of drought monitoring. Procedia Environmental Sciences
667 2011;3:32 –7. URL: <http://www.sciencedirect.com/science/article/pii/S1878029611000089>. doi:<https://doi.org/10.1016/j.proenv.2011.02.007>; 1st Conference on Spatial Statistics 2011 Mapping Global Change.
- 670 Sai F, Cumiskey L, Weerts A, Bhattacharya B, Haque Khan R. To-
671 wards impact-based flood forecasting and warning in bangladesh: a
672 case study at the local level in sirajganj district. Natural Hazards
673 and Earth System Sciences Discussions 2018;2018:1–20. URL: <https://www.nat-hazards-earth-syst-sci-discuss.net/nhess-2018-26/>.
674 doi:[10.5194/nhess-2018-26](https://doi.org/10.5194/nhess-2018-26).
- 676 Savitzky A, Golay MJE. Smoothing and Differentiation of Data by Sim-
677 plified Least Squares Procedures. Analytical Chemistry 1964;36(8):1627–
678 39. URL: <http://pubs.acs.org/doi/abs/10.1021/ac60214a047>. doi:[10.1021/ac60214a047](https://doi.org/10.1021/ac60214a047).

- 680 Schaaf C, Wang Z. MCD43A4 MODIS/Terra+Aqua BRDF/Albedo
681 Nadir BRDF Adjusted Ref Daily L3 Global - 500m V006 [Data
682 set]. 2015. URL: https://lpdaac.usgs.gov/dataset{_}discovery/modis/modis{_}products{_}table/mcd43a4{_}v006. doi:10.5067/MODIS/MCD43A4.006.
- 685 Stanke C, Kerac M, Prudhomme C, Medlock J, Murray V. Health effects of
686 drought: a systematic review of the evidence. PLoS currents 2013;5. URL:
687 <https://www.ncbi.nlm.nih.gov/pubmed/23787891>.
- 688 Stocker TF, Qin D, Plattner GK, Tignor M, Allen SK, Boschung J, Nauels A,
689 Xia Y, Bex V, Midgley PM, et al. Climate change 2013: The physical science
690 basis. 2013.
- 691 Tierney JE, Ummenhofer CC, deMenocal PB. Past and future rainfall in
692 the horn of africa. Science Advances 2015;1(9). URL: <https://advances.sciencemag.org/content/1/9/e1500682>. doi:10.1126/sciadv.1500682.
694 arXiv:<https://advances.sciencemag.org/content/1/9/e1500682.full.pdf>.
- 695 UNDP . KENYA ADAPTATION TO CLIMATE CHANGE IN ARID LANDS
696 (KACCAL) - KENYA CASE STUDY. Technical Report; 2013. URL: <http://gefonline.org/projectDetailsSQL.cfm?projID=3792>.
- 698 Upreti D, Huang W, Kong W, Pascucci S, Pignatti S, Zhou X, Ye H, Casa
699 R. A comparison of hybrid machine learning algorithms for the retrieval of
700 wheat biophysical variables from sentinel-2. Remote Sensing 2019;11(5). URL:
701 <http://www.mdpi.com/2072-4292/11/5/481>. doi:10.3390/rs11050481.
- 702 Venton CC, Fitzgibbon C, Shitarek T, Coulter L, Dooley O. The economics of
703 early response and disaster resilience: lessons from kenya and ethiopia. Final
704 report 2012;.

- 705 Vrieling A, Meroni M, Mude AG, Chantarat S, Ummenhofer CC, de Bie
706 KC. Early assessment of seasonal forage availability for mitigating the im-
707 pact of drought on east african pastoralists. *Remote Sensing of Environ-*
708 *ment* 2016;174:44 – 55. URL: <http://www.sciencedirect.com/science/article/pii/S0034425715302248>. doi:<https://doi.org/10.1016/j.rse.2015.12.003>.
- 711 WMO . Wmo guidelines on multi-hazard impact-based forecast and warning
712 services 2015;.
- 713 Yang H, Huntingford C. Brief communication. drought likelihood for east africa.
714 *Natural Hazards and Earth System Sciences* 2018;18(2):491–7.
- 715 Zambrano F, Vrieling A, Nelson A, Meroni M, Tadesse T. Prediction of drought-
716 induced reduction of agricultural productivity in chile from modis, rain-
717 fall estimates, and climate oscillation indices. *Remote Sensing of Environ-*
718 *ment* 2018;219:15 – 30. URL: <http://www.sciencedirect.com/science/article/pii/S0034425718304541>. doi:<https://doi.org/10.1016/j.rse.2018.10.006>.
- 721 Zargar A, Sadiq R, Naser B, Khan FI. A review of drought indices. *Environ-*
722 *mental Reviews* 2011;19(NA):333–49.
- 723 Zhang L, Jiao W, Zhang H, Huang C, Tong Q. Studying drought
724 phenomena in the continental united states in 2011 and 2012 using
725 various drought indices. *Remote Sensing of Environment* 2017;190:96
726 – 106. URL: <http://www.sciencedirect.com/science/article/pii/S0034425716304813>. doi:<https://doi.org/10.1016/j.rse.2016.12.010>.